NASA TECHNICAL NOTE

NASA TN D-8414

NASA TN D-8414

THREE-DIMENSIONAL FINITE-ELEMENT ANALYSIS OF FINITE-THICKNESS FRACTURE SPECIMENS

I. S. Raju and J. C. Newman, Jr.

Langley Research Center
Hampton, Va. 23665

NATIONAL AERONAUTICS AND SPACE ADMINISTRATION · WASHINGTON, D. C. · MAY 1977

1. Report No. NASA TN D-8414	2. Government Accession No.	3. Recipient's Catalog No.
4. Title and Subtitle THREE-DIMENSIONAL FINITE-ELEMENT ANALYSIS OF FINITE-THICKNESS FRACTURE SPECIMENS		5. Report Date May 1977 6. Performing Organization Code
7. Author(s) I. S. Raju and J. C. Newman, Jr.		8. Performing Organization Report No. L-10967
9. Performing Organization Name and Address NASA Langley Research Center Hampton, VA 23665		10. Work Unit No. 505-02-31-01 11. Contract or Grant No.
12. Sponsoring Agency Name and Address National Aeronautics and Space Administration Washington, DC 20546		13. Type of Report and Period Covered Technical Note 14. Sponsoring Agency Code

15. Supplementary Notes

I. S. Raju: NRC-NASA Resident Research Associate.

16. Abstract

The stress-intensity factors for most of the commonly used fracture specimens (center-crack tension, single- and double-edge-crack tension, and compact), those that have a through-the-thickness crack, were calculated using a three-dimensional finite-element elastic stress analysis. Three-dimensional singularity elements were used around the crack front. The stress-intensity factors along the crack front were evaluated by using a force method, developed herein, that requires no prior assumption of either plane stress or plane strain.

The calculated stress-intensity factors from the present analysis were compared with those from the literature whenever possible and were generally found to be in good agreement. The stress-intensity factors at the midplane for all specimens analyzed were within 3 percent of the two-dimensional plane-strain values. The stress-intensity factors at the specimen surfaces were considerably lower than at the midplanes. For the center-crack tension specimens with large thickness-to-crack-length ratios, the stress-intensity factor reached a maximum near the surface of the specimen. In all other specimens considered the maximum stress intensity occurred at the midplane.

17. Key Words (Suggested by Author(s))	18. Distribution Statement
Cracks Elasticity Fracture Stress-intensity factors Three-dimensional finite elements	Unclassified – Unlimited Subject Category 39

19. Security Classif. (of this report)	20. Security Classif. (of this page)	21. No. of Pages	22. Price*
Unclassified	Unclassified	40	$4.00

*For sale by the National Technical Information Service, Springfield, Virginia 22161

THREE-DIMENSIONAL FINITE-ELEMENT ANALYSIS OF FINITE-THICKNESS FRACTURE SPECIMENS

I. S. Raju* and J. C. Newman, Jr.
Langley Research Center

SUMMARY

The stress-intensity factors for most of the commonly used fracture specimens (center-crack tension, single- and double-edge-crack tension, and compact), those that have a through-the-thickness crack, were calculated using a three-dimensional finite-element elastic stress analysis. Three-dimensional singularity elements were used around the crack front. The stress-intensity factors along the crack front were evaluated by using a force method, developed herein, that requires no prior assumption of either plane stress or plane strain.

The calculated stress-intensity factors from the present analysis were compared with those from the literature whenever possible and were generally found to be in good agreement. The stress-intensity factors at the midplane for all specimens analyzed were within 3 percent of the two-dimensional plane-strain values. The stress-intensity factors at the specimen surfaces were considerably lower than at the midplanes. For the center-crack tension specimens with large thickness-to-crack-length ratios, the stress-intensity factor reached a maximum near the surface of the specimen. In all other specimens considered the maximum stress intensity occurred at the midplane.

INTRODUCTION

The stress-intensity factor concept has been used to correlate fatigue crack-growth rates and to determine fracture properties of engineering materials. For plane elastic continua containing cracks, the stress-intensity factors usually have been obtained from two-dimensional analyses assuming either plane stress or plane strain and, therefore, they are constant across the thickness (refs. 1 and 2). For fracture specimens of finite thickness, however, the stress-intensity factors vary along the crack front. Inasmuch as accurate stress-intensity factors are needed to correlate fatigue crack-growth rates or to determine fracture properties for finite-thickness fracture specimens, analyses that account for these stress-intensity variations are needed.

---

*NRC-NASA Resident Research Associate.

For three-dimensional elastic continua with cracks, the stress field near the crack front is obtained by the solution of the Navier's equations of equilibrium subjected to appropriate boundary conditions (ref. 3). Due to the complexity of the solution, however, the stress fields around the crack front in three-dimensional continua are available for only a few restricted classes of problems such as penny-shaped and elliptic cracks in an infinite solid (ref. 3). For fracture specimens of finite thickness with through-the-thickness cracks, some attempts (ref. 4) have been made to obtain the stress distribution close to the crack front, but the solutions have been found to be intractable in closed form (refs. 4 and 5). Even so, the form of the stress distribution near the crack front was obtained. Hartranft and Sih (ref. 4) showed that the stresses σ_x, σ_y, σ_z, and σ_{xy} had a square-root singularity at the crack front and the two transverse shear stresses σ_{yz} and σ_{xz} were finite throughout the plate.

In view of the difficulties in obtaining a closed-form analysis, several approximate three-dimensional methods, such as direct potential (refs. 6 and 7) and finite elements (refs. 8 to 10), have been used for the stress analysis of finite-thickness fracture specimens containing through-the-thickness cracks. Each solution from these references, however, was for a different specimen configuration, and the results cannot be directly compared. Further, most investigators have used the crack-opening displacements and the plane-strain assumption to evaluate the stress-intensity factor across the thickness. This approach is justified only near the middle of the specimen where the plane-strain conditions may exist, but not near the free surfaces of the specimen. Consequently, this approach may lead to errors in the stress-intensity factor near the specimen surface.

The purpose of this paper is to present a three-dimensional finite-element elastic stress analysis of the most commonly used fracture specimens (center-crack tension, single- and double-edge-crack tension, and compact). A three-dimensional singularity element in the shape of a pentahedron, similar to that developed by Tracey (ref. 8), was used at the crack front; however, herein a nodal force method was developed and was used to evaluate the mode I stress-intensity factors (ref. 1) along the crack front. This method, in contrast to the crack-opening displacement method, requires no prior assumptions of plane stress or plane strain. The accuracy of the nodal force method was verified by conducting two-dimensional analyses on center-crack, single-edge-crack, and double-edge-crack tension specimens.

In the present paper, the distributions of stress intensity (mode I) across the thickness for all of the fracture specimens previously mentioned were obtained. The effects of specimen thickness and specimen length on these distributions were investigated. These results were compared with existing stress-intensity factor solutions from the literature whenever possible.

SYMBOLS

Scalars:

b	half-width of specimen
c	crack length defined in figure 1
E	Young's modulus
F	stress-intensity boundary-correction factor
F_j	nodal force for node j
G	shear modulus
h	half-length of specimen
i,j	indices
K	stress-intensity factor
K_{ap}	apparent stress-intensity factor
p	applied load per unit thickness
r,θ	polar coordinates with origin at crack tip
R	distance from crack tip to point on Y = 0 and X = Constant plane (see fig. 5)
S	applied stress
t	thickness of specimen
u,v,w	displacement in x-, y-, and z-direction, respectively
x,y,z	local Cartesian coordinates

X,Y,Z global Cartesian coordinates

β_1,β_2 distances from crack front (see fig. 4)

ν Poisson's ratio

ξ,η,ζ orthogonal coordinates (parent system)

Matrices:

$[B]$ strain-displacement matrix

$[D]$ elasticity matrix $\langle\sigma\rangle = [D]\langle\epsilon\rangle$

$[J]$ Jacobian matrix

$[K]$ stiffness matrix of an element

$[n_i],[n_i']$ shape functions for an element

$\langle\tilde{u}\rangle$ generalized displacements $\langle\tilde{u}\rangle = \langle u\ v\ w\rangle$

$\langle\alpha\rangle$ constants

$\langle\delta\rangle$ column matrix of nodal displacements for an element

$\langle\epsilon\rangle$ strain matrix $\langle\epsilon_x\epsilon_y\epsilon_z\epsilon_{xy}\epsilon_{yz}\epsilon_{zx}\rangle$

$\langle\sigma\rangle$ stress matrix $\langle\sigma_x\sigma_y\sigma_z\sigma_{xy}\sigma_{yz}\sigma_{zx}\rangle$

ANALYSIS

Traditional finite-element analyses need large numbers of small elements around the crack tip to delineate the stress field satisfactorily. Several attempts, in two-dimensional analyses (refs. 11 to 13), have been made to develop a special element or elements that account for the stress and strain singularity. These elements are either based on the exact form of the stress field near the crack tip or include functions that simulate the square-root singularity of the stresses at the crack tip. Stress-intensity factors obtained using such elements are substantially more accurate than those based on

conventional finite elements (refs. 11 to 13); therefore, a three-dimensional singularity element was developed herein for the analysis of finite-thickness specimens with cracks. The specimens analyzed are shown in figure 1.

Three-Dimensional Analysis

Finite-element idealizations.- Three types of elements (isoparametric, singularity, and square-root) in combinations were used to model the finite-thickness specimens, and a typical finite-element model is shown in figure 2. This model idealizes one-eighth of the center-crack and double-edge-crack tension specimens and one-quarter of the single-edge-crack tension and compact specimens shown in figure 1. Across the thickness, various numbers of layers of elements with various thicknesses were used. Figure 2(a) shows a typical four-layer model with equal thickness layers. Isoparametric hexahedron (linear strain) elements were used everywhere except in the vicinity of the crack front. Around the crack front the model had 8 "singularity elements" and 32 "square-root elements" for each layer. The singularity elements had square-root terms in their assumed displacement distributions and therefore produced a singular stress field at the crack front. The singularity elements were located only at the crack front. The square-root elements also had a square-root term in their assumed displacement distribution; they were located near the crack front and around the singularity elements. The fine-mesh model shown in figures 2(a) and 2(b) had 432 elements, 625 nodes, and 1875 degrees of freedom. The medium- and coarse-mesh models, figures 2(c) and 2(d), will be discussed later.

Isoparametric element.- Consider an isoparametric hexahedron (ref. 14) with eight nodes in a local Cartesian coordinate system (x,y,z) and a unit cube with eight nodes in an orthogonal coordinate system (ξ,η,ζ) (hereinafter termed as parent) as shown in figures 3(a) and 3(b), respectively. A unit cube (ref. 14) is used in the parent system for simplicity. The mapping from the parent system to the local system is expressed as

$$\begin{bmatrix} x \\ y \\ z \end{bmatrix} = \begin{bmatrix} [N] & & \\ & [N] & \\ & & [N] \end{bmatrix} \langle \alpha \rangle \tag{1}$$

where $[N]$ is a row vector given by

$$[N] = [1, \xi, \eta, \zeta, \xi\eta, \eta\zeta, \zeta\xi, \xi\eta\zeta] \tag{2}$$

and

$$\langle \alpha \rangle = \langle \alpha_1, \alpha_2, \ldots, \alpha_{24} \rangle \tag{3}$$

If the constants $\langle \alpha \rangle$ are expressed in terms of the coordinates of the eight nodes in the local system, equation (1) can be rewritten as

$$\begin{bmatrix} x \\ y \\ z \end{bmatrix} = \sum_{i=1}^{8} n_i \begin{bmatrix} x_i \\ y_i \\ z_i \end{bmatrix} \tag{4}$$

where

$$n_i = \left(2\xi\xi_i - \xi_i - \xi + 1\right)\left(2\eta\eta_i - \eta_i - \eta + 1\right)\left(2\zeta\zeta_i - \zeta_i - \zeta + 1\right) \tag{5}$$

The terms ξ_i, η_i, and ζ_i are the coordinates of node i in the parent system, and the terms x_i, y_i, and z_i are the coordinates of node i in the local system. Equation (4) gives a one-to-one mapping of the parent system onto the local system.

The assumed displacement distribution for the isoparametric hexahedron element (ref. 14) in figure 3(a) is

$$\begin{bmatrix} u \\ v \\ w \end{bmatrix} = \begin{bmatrix} n_i & & \\ & n_i & \\ & & n_i \end{bmatrix} \langle \delta \rangle \tag{6}$$

where the shape functions n_i (i=1,8) are given by equation (5) and $\langle \delta \rangle$, the nodal displacement vector, is defined by

$$\langle \delta \rangle = \langle u_1, u_2, \ldots, u_8, v_1, v_2, \ldots, v_8, w_1, w_2, \ldots, w_8 \rangle \tag{7}$$

This element is a linear strain element.

Singularity element.- The singularity element used herein exhibits a square-root singularity in σ_x, σ_y, σ_z, and σ_{xy}, and the transverse shear stresses σ_{yz} and σ_{zx} are finite (ref. 4). This element is like that developed by Tracey (ref. 8). The formulation of the singularity element is like that used for the isoparametric hexahedron element except that nodes 1,5 and 2,6 of the hexahedron were coalesced to form the shape of a pentahedron. The singularity element is located at the crack front as shown in figure 3(c). The z-axis of the local coordinate system was directed along the crack front. The coalescence of the nodes at the crack front causes the constraints $\{\tilde{u}_1\} = \{\tilde{u}_5\}$ and $\{\tilde{u}_2\} = \{\tilde{u}_6\}$. Due to these constraints the constants α_3, α_6, α_{11}, α_{14}, α_{19}, and α_{22} of equation (1) vanished, and equation (4) was modified as

$$\begin{bmatrix} x \\ y \\ z \end{bmatrix} = \sum_{i=1}^{8} n_i' \begin{bmatrix} x_i \\ y_i \\ z_i \end{bmatrix} \tag{8}$$

where

$$\left.\begin{aligned} n_1' &= (1 - \xi)(1 - \zeta) & n_2' &= (1 - \xi)\zeta \\ n_3' &= \xi(1 - \eta)\zeta & n_4' &= \xi(1 - \eta)(1 - \zeta) \\ n_5' &= n_1' & n_6' &= n_2' \\ n_7' &= \xi\eta\zeta & n_8' &= \xi\eta(1 - \zeta) \end{aligned}\right\} \tag{9}$$

The displacement distributions for the singularity element were assumed as

$$\begin{bmatrix} u \\ v \\ w \end{bmatrix} = \begin{bmatrix} n_i & & \\ & n_i & \\ & & n_i' \end{bmatrix} \{\delta\} \tag{10}$$

The shape functions n_i (i=1,8) in equation (10) were obtained from equations (9) by replacing ξ by $\sqrt{\xi}$, so that the square-root functions for u and v would provide singular stresses at the crack tip. The functions n_i' (i=1,8) for the transverse displacement w are linear and are given by equations (9). These distributions ensure that all stresses are singular at the crack front except the two transverse shear stresses σ_{yz} and σ_{xz}.

Square-root element.- Because the displacements near the crack tip have a square-root distribution, several rings of elements around the singularity elements were assigned square-root shape functions. The shape functions for these hexahedron elements were obtained by replacing ξ with $\sqrt{\xi}$ in equation (2). The constraints $\{\tilde{u}_1\} = \{\tilde{u}_5\}$ and $\{\tilde{u}_2\} = \{\tilde{u}_6\}$ were not applied to this element. The local coordinate system for each square-root element was determined by its neighboring singularity element as shown in figure 4(a). Further, to maintain the square-root character near the crack front, these elements were mapped without translation in the radial direction (fig. 4(b)). The coordinate transformation for this element is given by equation (4) where

$$n_i = \frac{1}{(\beta_2 - \beta_1)^2}\Big[2\xi\xi_i + \beta_2^2 + \beta_1^2 - \xi(\beta_1 + \beta_2) - \xi_i(\beta_1 + \beta_2)\Big](2\eta\eta_i - \eta_i - \eta + 1)(2\zeta\zeta_i - \zeta_i - \zeta + 1) \tag{11}$$

Strains and stiffness matrix.- The strains in the elements, previously mentioned, are obtained from the displacement distributions as

$$\{\epsilon\} = [B]\{\delta\} \tag{12}$$

The procedures for evaluating the strains and the strain energy are discussed in the literature (ref. 14) and are not repeated here.

The stiffness matrix for any element is obtained by

$$[K] = \int_{vol} [B]^T [D] [B] \, dx \, dy \, dz \tag{13}$$

where $[D]$ is the elasticity matrix which relates stresses to strains. Because the strain-displacement matrix $[B]$ is in terms of the parent coordinates, a change of variable is needed. Thus,

$$[K] = \int_0^1 \int_0^1 \int_0^1 [B]^T [D][B] \det[J] \, d\xi \, d\eta \, d\zeta \tag{14}$$

for isoparametric and singular elements, and

$$[K] = \int_0^1 \int_0^1 \int_{\beta_1}^{\beta_2} [B]^T [D][B] \det[J] \, d\xi \, d\eta \, d\zeta \tag{15}$$

for the square-root elements. The Jacobian matrix $[J]$ in equations (14) and (15) was obtained from equations (4), (8), and (11) for the isoparametric, singular, and square-root elements, respectively.

For the pentahedron and hexahedron elements, the integrations in equations (14) and (15) were too complex in closed form and, thus, numerical integration (Gaussian) was used.

After the stiffness matrices of the elements in their local systems are obtained, the stiffness matrices in a convenient global system (X,Y,Z) are obtained by elementary coordinate transformations.

Stress-intensity factor.- The stress-intensity factor gives a measure of the magnitude of the stresses near the crack tip. In general, when the loading is complex, the stress-intensity factor depends on the three basic modes of deformation. Here only tension specimens were analyzed, however, and therefore only mode I deformations were considered. The mode I stress-intensity factor K is usually defined as

$$K = S\sqrt{\pi c}\, F \tag{16}$$

where S is an applied stress and F is the boundary-correction factor which accounts for the finiteness of the specimen.

The remainder of this section presents a force method, developed herein for evaluating stress-intensity factors. In this method, neither plane stress nor plane strain has to be assumed. The forces normal to the crack plane and ahead of the crack front were used to evaluate the stress-intensity factor.

Consider a specimen idealized by several layers as shown in figure 5. The forces normal to the $Y = 0$ plane along the junction line between layers i and $i+1$ are assumed to be contributed from the normal stresses acting over one-half of the layers on either side of the junction line (shaded area ABCD in fig. 5). The normal stress σ_Y at any point in the $Y = 0$ plane is assumed to be given by

$$\sigma_Y = \frac{K}{\sqrt{2\pi r}} + A_1' r^{1/2} + A_2' r^{3/2} + \ldots \tag{17}$$

where r is the distance from the crack front. In general, K and A_i' are functions of the coordinate Z. In the present analysis, however, K and A_i' were assumed to be constant over the shaded region ABCD in figure 5. This assumption is justified when the layers are thin.

The total force in the Y-direction acting over the shaded region ABCD (fig. 5) is given by

$$F_Y = \int_0^R \sigma_Y \, dr\left(\frac{t_i + t_{i+1}}{2}\right) \tag{18}$$

Substituting equation (17) into equation (18) gives

$$F_Y = \left[\frac{K}{\sqrt{2\pi}}\left(2\sqrt{R}\right) + A_1 R^{3/2} + A_2 R^{5/2} + \ldots\right]\left(\frac{t_i + t_{i+1}}{2}\right) \tag{19}$$

where A_i represents constants. Using only the first term on the right-hand side of equation (19), K is replaced by the apparent stress-intensity factor K_{ap} (ref. 15) and is evaluated as

$$F_Y = \frac{K_{ap}}{\sqrt{2\pi}} \sqrt{R}\left(t_i + t_{i+1}\right) \tag{20}$$

The force F_Y was obtained from the finite-element analysis and was determined as follows. Let nodes $j, j+1, \ldots, j+4$ be the nodes lying on the junction line between layers i and $(i+1)$ and for $0 \leq r \leq R$; the finite-element analysis gives the nodal forces in the Y-direction at all of these nodes. Let the forces be $F_j, F_{j+1}, \ldots, F_{j+4}$. Thus, the total force over a distance R is

$$F_Y = F_j + F_{j+1} + F_{j+2} + F_{j+3} + F_{j+4}' \tag{21}$$

where F_{j+4}', the nodal force at node $j+4$, is calculated using only the elements that are connected to node $j+4$ and are inside the shaded region ABCD (see fig. 5). For various values of R, the number of nodal forces contributing to F_Y would also vary.

The total force F_Y obtained from the finite-element analysis is substituted into equation (20), and the apparent stress-intensity factor K_{ap} is evaluated. The procedure is repeated for various values of R. Equating equations (19) and (20) gives

$$K_{ap} = K + B_1 R + B_2 R^2 + \ldots \tag{22}$$

where B_i represents constants. From equation (22), a plot of K_{ap} against R is linear for small values of R and the intercept at R = 0, at the crack front, gives the stress-intensity factor at a particular location along the crack front. The procedure is repeated at various locations (Z) along the crack front.

Two-Dimensional Analysis

In order to establish the validity of both the singularity element and the calculation of the stress-intensity factor using the force method, two-dimensional finite-element analyses were conducted on center-crack tension (CCT), double-edge-crack tension (DECT), and single-edge-crack tension (SECT) specimens (fig. 1). Only one layer of three-dimensional elements was used in the two-dimensional analyses. To simulate plane-strain conditions, the displacements in the Z-direction were prescribed to be zero at all nodes.

Finite-element idealization.- Coarse, medium, and fine meshes were used to idealize the two-dimensional specimens to study convergence of the solution. The fine-mesh idealization (figs. 2(a) and 2(b)) had 108 elements, 250 nodes, and 750 degrees of freedom. The medium-mesh idealization (figs. 2(a) and 2(c)) had 92 elements, 214 nodes, and 642 degrees of freedom. The coarse-mesh idealization (figs. 2(a) and 2(d)) had 68 elements, 160 nodes, and 480 degrees of freedom. Figure 2 also shows the element patterns in the crack-tip region for the three meshes.

Stress-intensity factor.- The stress-intensity factor in the two-dimensional analysis was evaluated by the force method. As only one layer was used across the thickness, equation (20) becomes

$$F_Y = K_{ap}\sqrt{\frac{R}{2\pi}}\,t \tag{23}$$

where t is the thickness of the specimen. The remainder of the analysis was identical to the three-dimensional analysis; equations (21) and (22) were used to compute F_Y and to evaluate the stress-intensity factors.

RESULTS AND DISCUSSION

The stress-intensity factors for the specimens shown in figure 1 were calculated herein using either a two- or a three-dimensional finite-element analysis. Two-dimensional analyses were used to verify the force method for calculating the stress-intensity factors. In the three-dimensional analyses, the effects of specimen thickness and specimen length on the variation of stress intensity along the crack front were studied. The stress-intensity factors from the present analysis were compared with other solutions whenever possible (refs. 6 to 10).

Two-Dimensional Results

The stress-intensity factors obtained from the force method for two-dimensional analysis are presented in table I for CCT, DECT, and SECT specimens. Each of the three specimen types had a c/b ratio of 0.5. Stress-intensity factors from the literature are also given in table I.

Figure 6 shows the apparent stress-intensity factor for the CCT specimen obtained by the force method plotted against the distance R/c for all three meshes. For the fine mesh (triangular symbols) this figure shows a straight-line relationship between the apparent stress-intensity factor K_{ap} and the distance from the crack tip R except for the K_{ap} value closest to the crack tip, $R = 0$. The K_{ap} value closest to the crack tip was calculated from the force contributions from the singularity elements only. These elements were stiffer than other elements and therefore attracted larger force. At larger distances from the crack tip, however, the square-root elements adjusted the forces F_Y so that a straight-line relationship between K_{ap} and R/c was maintained. If the K_{ap} value nearest the crack tip is neglected, the slope of the straight line of the fine mesh is very nearly equal to the slope obtained from Newman's collocation results (ref. 16) (circular symbols, fig. 6). The K_{ap} value closest to the crack tip was therefore neglected in the present application of the force method.

The medium-mesh model (square symbols, fig. 6) gave a stress-intensity factor closer to the collocation results (ref. 16) than either the coarse-mesh model (diamond symbols) or the fine-mesh model (triangular symbols). All three meshes, however, gave stress-intensity factors within 2.5 percent of the collocation results. Since the slope of the straight line from the fine-mesh results is in good agreement with the slope from Newman's collocation results, the fine-mesh model gave the same stress distribution in the crack-tip region as the collocation results but the magnitude of the stresses was slightly lower than that from the collocation results.

The stress-intensity factors obtained using the force method (table I) agree within -1.4, -0.12, and -4.7 percent for the CCT, DECT, and SECT specimens, respectively, compared with the generally accepted values given in references 1 and 16.

In general, the force method gave stress-intensity factors which were in good agreement with those from the literature. Because the fine-mesh model gave good stress-intensity factors for all three specimens considered, this mesh was also used in the three-dimensional analysis.

Three-Dimensional Results

Center-crack tension specimen.- In the following sections the effects of specimen thickness and specimen length on stress-intensity variations across the thickness are presented. These results are compared with existing stress-intensity factor solutions from the literature whenever possible. Also, the stress-intensity variation in the boundary layer (layer at the intersection of the crack and the free surface) is studied in detail.

Thickness effect: A thin center-crack tension specimen (fig. 1(a)) with $\frac{h}{b} = 0.5$, $\frac{c}{b} = 0.5$, and $\frac{t}{c} = 0.5$ was analyzed. This specimen configuration was selected because it was also analyzed by Atluri and Kathiresan (ref. 10), who used a singularity element derived from a hybrid displacement model. The present finite-element model had four nonuniform layers across the half thickness. The outer layers, near the surface, were made an order of magnitude thinner than the inner layers. The layer thicknesses from the midplane to the surface were 0.266t, 0.167t, 0.05t, and 0.017t. This four-layer model was termed the nonuniform-layer model.

Stress-intensity factors obtained from the present analysis and those from reference 10 are compared in figure 7. The results agree well (within 5 percent) with each other. The stress-intensity factors are nearly constant over most of the thickness but are lower near the surface. The stress-intensity factor at the midplane is nearly equal to the plane-strain value (ref. 17) shown by the dashed line.

A center-crack tension specimen thicker than that considered previously was also analyzed. This specimen had $\frac{h}{b} = 0.875$, $\frac{c}{b} = 0.5$, and $\frac{t}{c} = 3$. In the present analysis of this specimen, the number of layers (equal thickness) across the thickness was systematically varied from two to five. Results based on layers of equal thickness were then compared in figure 8 with results from the nonuniform-layer model. For layers of equal thickness the nondimensional crack-opening displacements are presented in table II and were found to be insensitive to the number of layers. Similarly, table III and figure 8 show that the stress-intensity factors were insensitive to the number of layers and at the midplane they were about 2 percent lower than the plane-strain value (dashed line). The stress-intensity factors have a peak value near the surface $\left(\frac{Z}{t} \approx 0.4\right)$, but the lowest value occurs at the surface.

Boundary-layer effect: Hartranft and Sih (ref. 18) proposed that the stress-intensity factors in the interior of a specimen were nearly equal to the plane-strain value, but, in a very thin "boundary layer" near the free surface, the stress-intensity factors "drop off" rapidly and equal zero at the surface. To investigate the boundary-layer effect, the nonuniform-layer model was used. The results obtained from the nonuniform-layer model are shown in figure 8 (diamond symbols). These results show that the stress-intensity is about 10 percent lower at the free surface than the previous results (two to five equal-thickness layers). The stress intensity in the interior of the specimen was the same for all models.

To study the boundary-layer effect further, the apparent stress-intensity factors K_{ap} obtained using the force method and the nonuniform-layer model are plotted against R/c in figure 9 for various values of Z/t. As in the two-dimensional analysis, the results from the three-dimensional analysis show the straight-line relationship (as proposed by eq. (22)) for small values of R/c. For each value of Z/t, a straight line was fitted (by the method of least squares) to the K_{ap} results to evaluate the stress-intensity factor. As previously discussed, the K_{ap} value closest to the crack front was neglected. As in the two-dimensional analysis the intercept of these lines at $\frac{R}{c} = 0$ gives the stress-intensity factor. The stress-intensity factors obtained at $\frac{R}{c} = 0$ from figure 9 are given in table III.

The slopes of the straight lines for $\frac{Z}{t} = 0$, 0.266, and 0.433 are nearly the same. However, for $\frac{Z}{t} = 0.483$ and 0.5 (the layers close to the surface) significantly different slopes are observed, suggesting a highly localized boundary-layer effect. The results of the present analysis showed that significantly different slopes of the straight line occurred in a region $0.483 \leqq \frac{Z}{t} \leqq 0.5$, that is, in a layer of 0.017t near the surface. In reference 18, the boundary-layer thickness was estimated to be $t\Big/\left(4 + \frac{16t}{c}\right)$. This estimate corresponds to a boundary-layer thickness of 0.02t for the CCT specimen with $\frac{t}{c} = 3$. The size of the boundary layer from the present analysis is in good agreement with the predictions from reference 18. For the two CCT specimens considered the boundary-layer thicknesses were estimated using reference 18 and are shown in figures 7 and 8.

At the surface $\left(\frac{Z}{t} = 0.5\right)$, the plot of K_{ap} against R/c deviated from the straight-line relationship (fig. 9). This behavior suggests that the singularity at the surface of the specimen may be different from the classical square-root singularity. Folias (ref. 19) has shown that the stresses close to the crack front are proportional to $r^{-\left(\frac{1}{2}+2\nu\right)}$ and displacements close to the crack front are proportional to $r^{\frac{1}{2}-2\nu}$. Thus, the displace-

ments at the crack front for Poisson's ratio greater than 1/4 are singular. He proposed that linear elastic theory may be inadequate to predict the actual behavior at the surface. The literature contains no accepted mathematical proof to determine the order of the singularity where the crack meets the surface.

The stress-intensity factors from the present results (shown in fig. 8) increased monotonically from the middle of the specimen to a peak near $\frac{Z}{t} = 0.4$ and dropped off rapidly in the boundary layer. This type of behavior was termed "peaking." To investigate the peaking behavior in the stress-intensity variation across the thickness, four thickness-to-crack-length ratios $\left(\frac{t}{c} = 1, 2, 3, \text{ and } 4\right)$ were analyzed with $\frac{h}{b} = 0.875$ and $\frac{c}{b} = 0.5$. The nonuniform-layer model was used, and the results are shown in figure 10. The peaking behavior was not observed for $\frac{t}{c} = 1$ but occurred for all other thickness-to-crack-length ratios. The peaking behavior was most pronounced for the largest value of t/c considered. The reasons for this peaking behavior are not understood at present.

Specimen-length effect: In the laboratory, specimen lengths are usually longer than the length considered in previous examples; therefore, to investigate the effects of specimen length on stress-intensity distributions, the stress intensity was calculated by using the nonuniform-layer model for a CCT specimen with $\frac{h}{b} = 3$ and $\frac{t}{c} = 3$. The stress-intensity factors obtained are given in table IV. Figure 10 shows the distribution of stress-intensity factors across the thickness for $\frac{h}{b} = 0.875$ and for $\frac{h}{b} = 3$ (triangular symbols). As expected, the longer specimen had lower stress-intensity factors than the short specimen. The specimen with $\frac{h}{b} = 3$ also showed the peaking behavior.

Double-edge-crack tension specimen.- A double-edge-crack tension specimen as shown in figure 1(b) with $\frac{h}{b} = 0.875$, $\frac{c}{b} = 0.5$, and $\frac{t}{c} = 3$ was analyzed. Again the nonuniform-layer model was used. Table V gives the stress-intensity factors and table VI gives the nondimensional crack-opening displacements. Figure 11 shows the variation of stress-intensity factor across the thickness (triangular symbols) from the present analysis. The stress-intensity factors were nearly uniform for most of the specimen thickness but, again, were lower at the surface. However, these results do not show the peaking behavior that was observed in the CCT specimen for the same thickness-to-crack-length ratio.

In order to investigate the peaking behavior in the DECT specimen, two specimens with $\frac{h}{b} = 3$ and $\frac{t}{c} = 3$ or 9 were analyzed. The results in figure 11 (lower curves) showed that these specimens exhibited no peaking; however, peaking may occur in DECT specimens provided the t/c ratio is large enough.

Single-edge-crack tension specimen.- Single-edge-crack tension specimens (SECT) as in figure 1(c) with $\frac{h}{b} = 1.75$ and 6, $\frac{c}{b} = 1.0$, and $\frac{t}{c} = 3$ were analyzed. Again the

nonuniform-layer model was used in the analysis. Table VII gives the stress-intensity factors across the thickness for the two specimen lengths. Figure 12 shows the variation of the stress-intensity factor across the thickness. As in the DECT configuration, the stress-intensity factors are nearly uniform over most of the thickness and are lower than the midplane value near the free surface. The stress-intensity factor at the middle of the specimen was within 1 percent of the plane-strain value (dashed line) (ref. 1). The stress-intensity factors were nearly the same for the two specimen lengths.

Compact specimen.- The compact specimen (fig. 1(d)) is much like the SECT specimen except that the loading is applied at the crack mouth. This specimen configuration with $\frac{h}{b} = 1$, $\frac{c}{b} = 1$, and $\frac{t}{c} = 1$ was also analyzed by Tracey (ref. 8). He used a singularity element like that developed in this report but incorporating a much finer mesh around the crack front. Reference 8 used two methods to evaluate the stress-intensity factor: (a) a crack-opening displacement method (with plane-strain assumption) and (b) a local stress method.

Table VIII gives the stress-intensity factors across thickness for the compact specimen, and figure 13 compares these results with those from reference 8. As expected, near the surface the present results do not agree with the results from reference 8 based on the crack-opening displacement method because of the assumption of plane strain. The present results agree very well, however, with the local stress-method results of reference 8, although the present analysis used only 4 elements across the thickness compared with 15 elements used in reference 8. This close correlation indicates that the force method yields reliable results.

In order to investigate the thickness effect, a compact specimen with the same configuration as previously considered, but with a larger thickness ratio $\left(\frac{t}{c} = 2\right)$, was also analyzed. The same mesh was used except that the Z-coordinates were scaled up by a factor of 2. The results for this case are presented in table VIII and figure 14. The stress-intensity factor at the free surface was about 0.65 of the value at the midplane of the specimen. Tracey (ref. 8) also analyzed this configuration and found that this ratio was about 0.7 (triangular symbol). Tracey's results, however, were obtained using crack-opening displacements with the plane-strain assumption. When he assumed a plane-stress condition at the free surface, the ratio was 0.64 (square symbol), which agrees well with the present results.

The present analysis showed that for a specimen with $\frac{t}{c} = 2$ (fig. 14) the stress-intensity factor at the free surface was only about 4 percent lower than the corresponding value for the specimen with $\frac{t}{c} = 1$ (fig. 13). For both thicknesses, the stress-intensity factors at the middle of the plate were within 1 percent of the plane-strain value (ref. 6).

CONCLUDING REMARKS

The stress-intensity factors for most of the commonly used fracture specimens (center-crack tension, single- and double-edge-crack tension, and compact) with through-the-thickness cracks were calculated using a three-dimensional finite-element elastic stress analysis. Three-dimensional singularity elements in the shape of pentahedrons were used at the crack front. A force method which requires no prior assumption of either plane stress or plane strain was developed and used to evaluate the stress-intensity factors across the thickness for these specimens.

For all specimen types considered, the calculated stress-intensity factor at the midplane of the specimen was within 3 percent of the plane-strain (two-dimensional) value. The stress-intensity factors at the surface of the specimens were considerably lower (10 to 35 percent) than the midplane values. The stress-intensity factors near the surface of the specimens fell off rapidly in a small "boundary layer." The calculated thickness of this boundary layer from the present analysis was in good agreement with that proposed in the literature. The present results also indicated that the crack-tip singularity at the surface of the specimen may be different from the classical square-root singularity.

In the center-crack tension specimen the maximum stress-intensity factor near the specimen surface was about 5 to 10 percent higher than the midplane value but at the surface it was up to 10 percent lower than the midplane value. This "peaking" in the stress-intensity factor near the surface was most pronounced for the largest thickness-to-crack-length ratio considered (2 to 1). The peaking behavior was not observed for the single-edge-crack, double-edge-crack, and compact specimens.

The specimen length had a strong influence on the magnitude of the stress-intensity factor but had no appreciable effect on its distribution across the thickness. The shorter-length specimens had higher stress-intensity factors than the longer-length specimens.

The stress-intensity factors from the present analyses were in good agreement (5 percent) with the stress-intensity factors from the literature. The stress-intensity factors obtained herein may be used to correlate fatigue crack-growth rates and to determine fracture properties of finite-thickness fracture specimens. The present three-dimensional analysis shows that the plane-strain stress-intensity factors for the center-crack tension and double-edge-crack tension specimens may be sufficient for correlating fatigue-crack growth rates and fracture properties because of the small variations in the

stress intensity across the thickness. For the single-edge-crack and compact specimens, however, the plane-strain values may not be sufficient because of large variation in the stress intensity across the thickness.

Langley Research Center
National Aeronautics and Space Administration
Hampton, VA 23665
February 9, 1977

REFERENCES

1. Paris, Paul C.; and Sih, George C.: Stress Analysis of Cracks. Fracture Toughness Testing and Its Applications, Spec. Tech. Publ. No. 381, American Soc. Testing Mater., c.1965, pp. 30-83.

2. Williams, M. L.: On the Stress Distribution at the Base of a Stationary Crack. Trans. ASME, Ser. E: J. Appl. Mech., vol. 24, no. 1, Mar. 1957, pp. 109-114.

3. Kassir, M. K.; and Sih, G. C.: Three-Dimensional Stress Distribution Around an Elliptical Crack Under Arbitrary Loadings. Trans. ASME, Ser. E: J. Appl. Mech., vol. 33, no. 3, Sept. 1966, pp. 601-611.

4. Hartranft, R. J.; and Sih, G. C.: The Use of Eigenfunction Expansions in the General Solution of Three-Dimensional Crack Problems. J. Math. & Mech., vol. 19, no. 2, Aug. 1969, pp. 123-138.

5. Sih, G. C.: A Review of the Three-Dimensional Stress Problem for a Cracked Plate. Int. J. Fract. Mech., vol. 7, no. 1, Mar. 1971, pp. 39-61.

6. Cruse, T. A.; and Vanburen, W.: Three-Dimensional Elastic Stress Analysis of a Fracture Specimen With an Edge Crack. Int. J. Fract. Mech., vol. 7, no. 1, Mar. 1971, pp. 1-15.

7. Cruse, T. A.: Lateral Constraint in a Cracked, Three Dimensional Elastic Body. Int. J. Fract. Mech., vol. 6, no. 3, Sept. 1970, pp. 326-328.

8. Tracey, D. M.: Finite Elements for Three-Dimensional Elastic Crack Analysis. Nucl. Eng. & Des., vol. 26, no. 2, 1974, pp. 282-290.

9. Barsoum, Roshdy S.: On the Use of Isoparametric Finite Elements in Linear Fracture Mechanics. Int. J. Numer. Methods Eng., vol. 10, no. 1, 1976, pp. 25-37.

10. Atluri, S.; and Kathiresan, K.: An Assumed Displacement Hybrid Finite Element Model for Three-Dimensional Linear-Fracture-Mechanics Analysis. Proceedings 12th Annual Meeting of the Society of Engineering Science, 1975, pp. 391-399.

11. Tracey, D. M.: Finite Elements for Determination of Crack Tip Elastic Stress Intensity Factors. Eng. Fract. Mech., vol. 3, Oct. 1971, pp. 255-265.

12. Raju, I. Sanyasi: Finite Element Analysis for Stress Concentrations and Singularities. Ph. D. Thesis, Indian Inst. Sci. (Bangalore), 1972.

13. Wilson, W. K.: Finite Element Methods for Elastic Bodies Containing Cracks. Methods of Analysis and Solutions of Crack Problems. Volume 1 of Mechanics of Fracture, George C. Sih, ed., Noordhoff Int. Pub. (Leyden), c.1973, pp. 484-515.

14. Zienkiewicz, O. C.: The Finite Element Method in Engineering Science. McGraw-Hill Book Co., Inc., c.1971, pp. 129-153.

15. Smith, C. William: Use of Three-Dimensional Photoelasticity and Progress in Related Areas. Experimental Techniques in Fracture Mechanics, 2, SESA Monogr. No. 2, c.1975, pp. 3-58.

16. Newman, J. C., Jr.: An Improved Method of Collocation for the Stress Analysis of Cracked Plates With Various Shaped Boundaries. NASA TN D-6376, 1971.

17. Tada, Hiroshi; Paris, Paul C.; and Irwin, George R.: The Stress Analysis of Cracks Handbook. Del Research Corp., c.1973.

18. Hartranft, R. J.; and Sih, G. C.: An Approximate Three-Dimensional Theory of Plates With Application to Crack Problems. Int. J. Eng. Sci., vol. 8, no. 8, Aug. 1970, pp. 711-729.

19. Folias, E. S.: On the Three Dimensional Theory of Cracked Plates. Trans. ASME, Ser. E: J. Appl. Mech., vol. 42, no. 3, Sept. 1975, pp. 663-674.

TABLE I.- COMPARISON OF STRESS-INTENSITY FACTORS

FROM TWO-DIMENSIONAL ANALYSES

$\left[\frac{c}{b} = 0.5; \quad \frac{h}{b} = 3\right]$

Specimen	$K/S\sqrt{\pi c}$			
	Present results			Results from the literature
	Coarse mesh (a)	Medium mesh (b)	Fine mesh (c)	
CCT	1.160	1.174	1.170	[d]1.187
DECT	1.125	1.154	1.149	[e]1.151
SECT	2.680	2.702	2.687	[e]2.820

[a]68 elements, 160 nodes, and 480 degrees of freedom.

[b]92 elements, 214 nodes, and 642 degrees of freedom.

[c]108 elements, 250 nodes, and 750 degrees of freedom.

[d]Collocation (ref. 16).

[e]Conformal mapping (ref. 1).

TABLE II.- NONDIMENSIONAL CRACK-OPENING DISPLACEMENTS

FOR CCT SPECIMEN ON $Y = 0$ AND $X = -c$

$$\left[\frac{h}{b} = 0.875;\ \frac{c}{b} = 0.5;\ \frac{t}{c} = 3;\ \nu = \frac{1}{3}\right]$$

Distance from crack tip, r/c	Ev/Sc							
	2 layers		3 layers		4 layers		5 layers	
	$Z = 0$	$Z = \frac{t}{2}$	$Z = 0$	$Z = \frac{t}{2}$	$Z = 0$	$Z = \frac{t}{2}$	$Z = 0$	$Z = \frac{t}{2}$
0.0132	0.395	0.433	0.398	0.431	0.399	0.429	0.399	0.427
.0264	.558	.612	.562	.612	.562	.610	.563	.608
.04	.685	.754	.690	.755	.691	.755	.691	.754
.08	.962	1.069	.968	1.076	.969	1.080	.970	1.083
.12	1.167	1.306	1.173	1.320	1.175	1.328	1.176	1.334
.16	1.338	1.507	1.345	1.527	1.347	1.539	1.348	1.548
.2	1.483	1.680	1.490	1.704	1.492	1.719	1.494	1.730
.4	1.980	2.283	1.989	2.322	1.993	2.343	1.995	2.356
.6	2.296	2.673	2.307	2.719	2.312	2.741	2.318	2.753
.8	2.469	2.886	2.480	2.935	2.486	2.956	2.488	2.968
1.0	2.517	2.946	2.529	2.995	2.534	3.016	2.537	3.027

TABLE III.- STRESS-INTENSITY BOUNDARY-CORRECTION FACTORS ACROSS THICKNESS FOR CCT SPECIMEN

$\left[\frac{h}{b} = 0.875;\ \frac{c}{b} = 0.5;\ \frac{t}{c} = 3;\ \nu = \frac{1}{3}\right]$

2 layers		3 layers		4 layers		4 layers (a)		5 layers	
Z/t	F (b)	Z/t	F (b)	Z/t	F (b)	Z/t	F (b)	Z/t	F (b)
0	1.394	0	1.393	0	1.394	0	1.401	0	1.394
.25	1.430	.166	1.409	.125	1.402	.266	1.433	.1	1.399
.5	1.474	.333	1.457	.25	1.429	.433	1.482	.2	1.416
		.5	1.480	.375	1.474	.483	1.439	.3	1.446
				.5	1.477	.5	1.316	.4	1.486
								.5	1.472

[a] Layers are of unequal thickness. Very thin layers were used at the surface.

[b] $F = \frac{K}{S\sqrt{\pi c}}$.

TABLE IV.- STRESS-INTENSITY BOUNDARY-CORRECTION FACTORS ACROSS THICKNESS FOR CCT SPECIMEN

$\left[\frac{c}{b} = 0.5; \quad \frac{t}{c} = 3; \quad \nu = \frac{1}{3}\right]$

Z/t	F (a)	
	$\frac{h}{b} = 0.875$	$\frac{h}{b} = 3$
0	1.401	1.197
.266	1.433	1.216
.433	1.482	1.243
.483	1.439	1.203
.5	1.316	1.102

[a] $F = \frac{K}{S\sqrt{\pi c}}$.

TABLE V.- STRESS-INTENSITY BOUNDARY-CORRECTION FACTORS ACROSS THICKNESS FOR DECT SPECIMEN

$\left[\frac{c}{b} = 0.5; \quad \frac{t}{c} = 3; \quad \nu = \frac{1}{3}\right]$

Z/t	F (a)	
	$\frac{h}{b} = 0.875$	$\frac{h}{b} = 3$
0	1.496	1.213
.266	1.470	1.204
.433	1.399	1.173
.483	1.281	1.099
.5	1.138	.991

[a] $F = \frac{K}{S\sqrt{\pi c}}$.

TABLE VI.- NONDIMENSIONAL CRACK-OPENING DISPLACEMENTS FOR DECT SPECIMEN ON Y = 0 AND X = -c

$\left[\frac{h}{b} = 0.875;\ \frac{c}{b} = 0.5;\ \frac{t}{c} = 3;\ \nu = \frac{1}{3}\right]$

Distance from crack tip, r/c	Ev/Sc	
	Z = 0	$Z = \frac{t}{2}$
0.0132	0.432	0.372
.0264	.612	.532
.04	.753	.662
.08	1.065	.960
.12	1.303	1.198
.16	1.506	1.406
.2	1.681	1.590
.4	2.373	2.318
.6	2.928	2.896
.8	3.408	3.378
1.0	3.866	3.825

TABLE VII.- STRESS-INTENSITY BOUNDARY-CORRECTION FACTORS ACROSS THICKNESS FOR SECT SPECIMEN

$\left[\frac{c}{b} = 1; \quad \frac{t}{c} = 3; \quad \nu = \frac{1}{3}\right]$

Z/t	F (a)	
	$\frac{h}{b} = 1.75$	$\frac{h}{b} = 6$
0	2.787	2.776
.266	2.764	2.757
.433	2.660	2.662
.483	2.434	2.441
.5	2.153	2.161

$$^{a}F = \frac{K}{S\sqrt{\pi c}}.$$

TABLE VIII.- STRESS-INTENSITY BOUNDARY-CORRECTION FACTORS ACROSS THICKNESS FOR COMPACT SPECIMEN

$\left[\frac{h}{b} = 1; \quad \frac{c}{b} = 1; \quad \nu = 0.3\right]$

Z/t	F (a)	
	$\frac{t}{c} = 1$	$\frac{t}{c} = 2$
0	7.967	7.958
.266	7.756	7.701
.433	7.158	6.963
.483	6.342	6.053
.5	5.361	5.167

$$^{a}F = \frac{K}{p\sqrt{\pi c/2b}}.$$

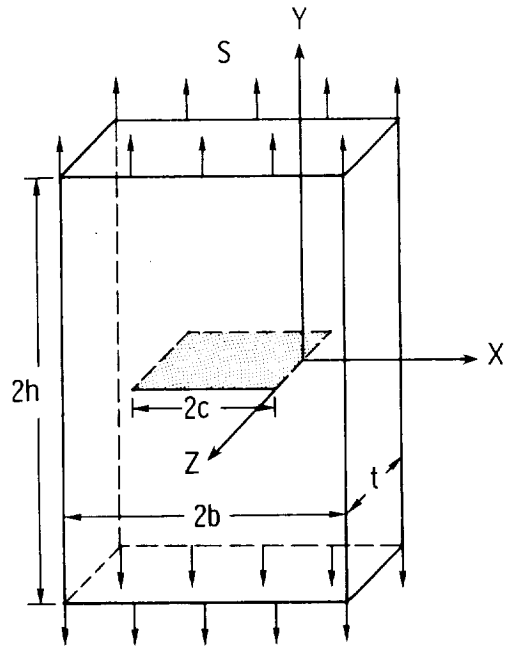

(a) Center crack tension (CCT).

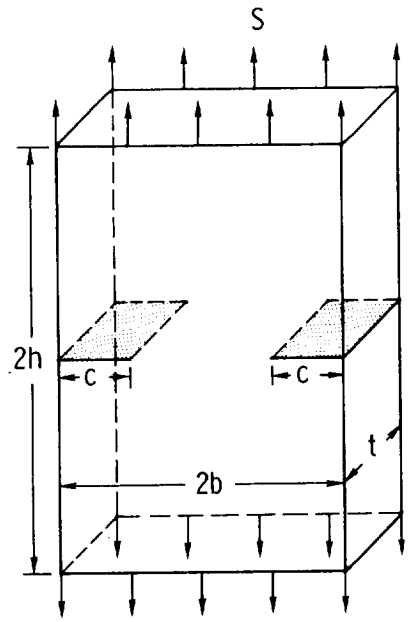

(b) Double-edge-crack tension (DECT).

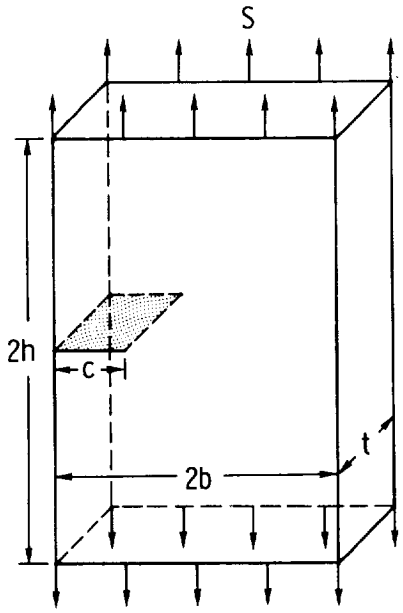

(c) Single-edge-crack tension (SECT).

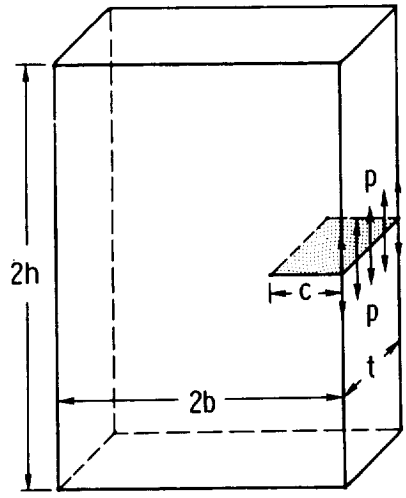

(d) Compact (CS).

Figure 1.- Fracture specimens.

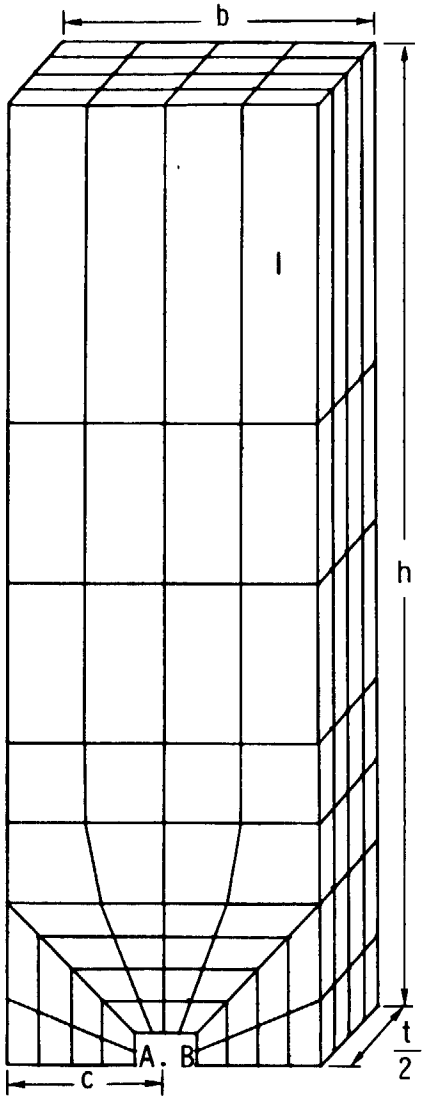

(a) Specimen model.

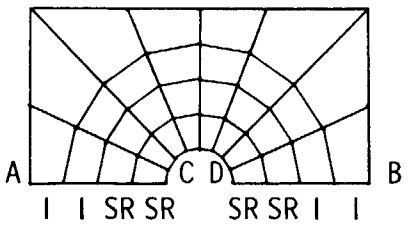

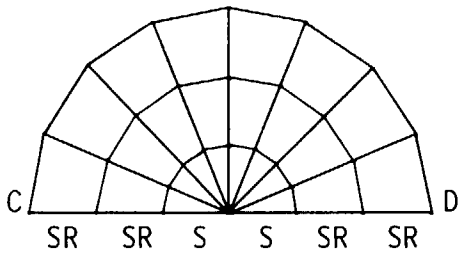

S Singularity element
SR Square-root element
I Isoparametric element

(b) Fine mesh.

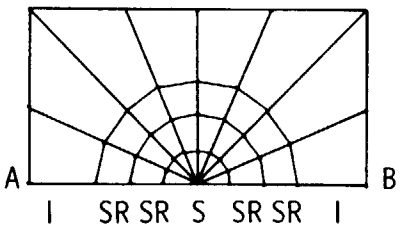

(c) Medium mesh.

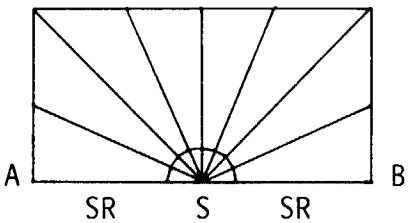

(d) Coarse mesh.

Figure 2.- Finite-element model.

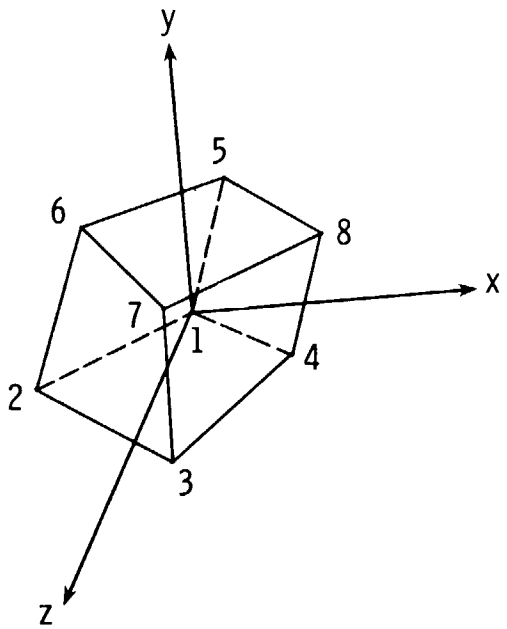

(a) Hexahedron in local coordinate system.

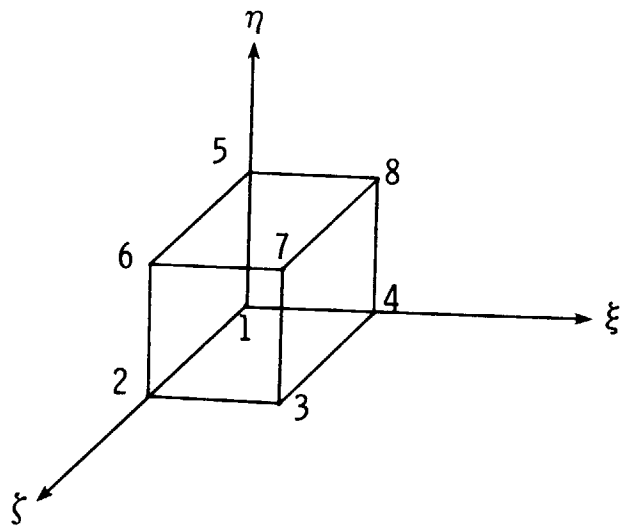

(b) Unit cube in parent coordinate system.

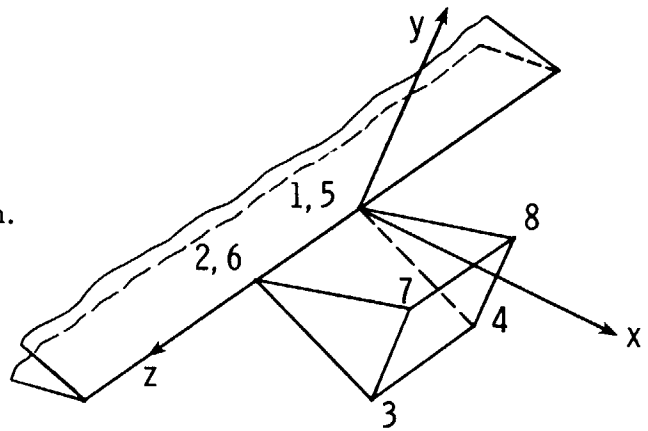

(c) Pentahedron in local coordinate system.

Figure 3.- Coordinate and element transformations.

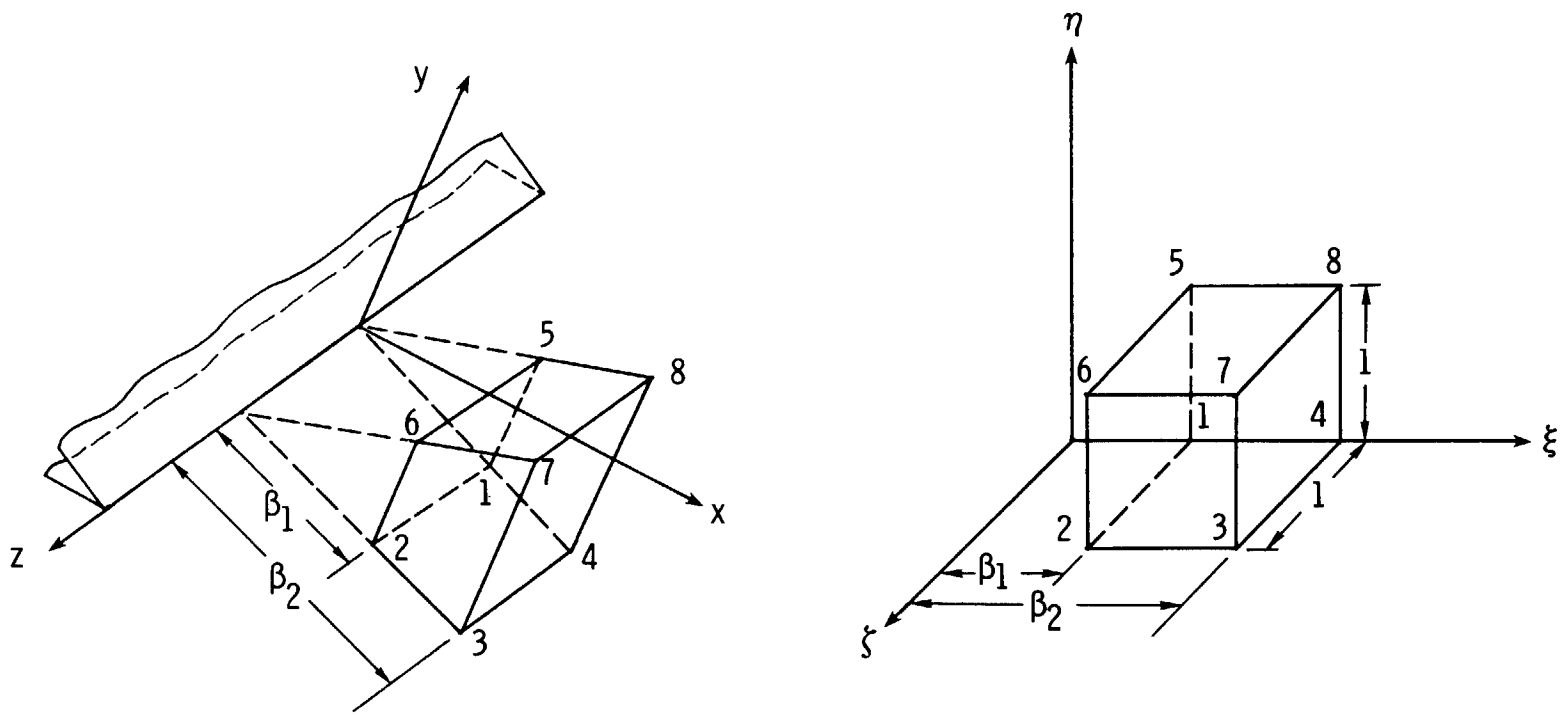

(a) Local system.

(b) Parent system.

Figure 4.- Coordinate and element transformations for square-root elements.

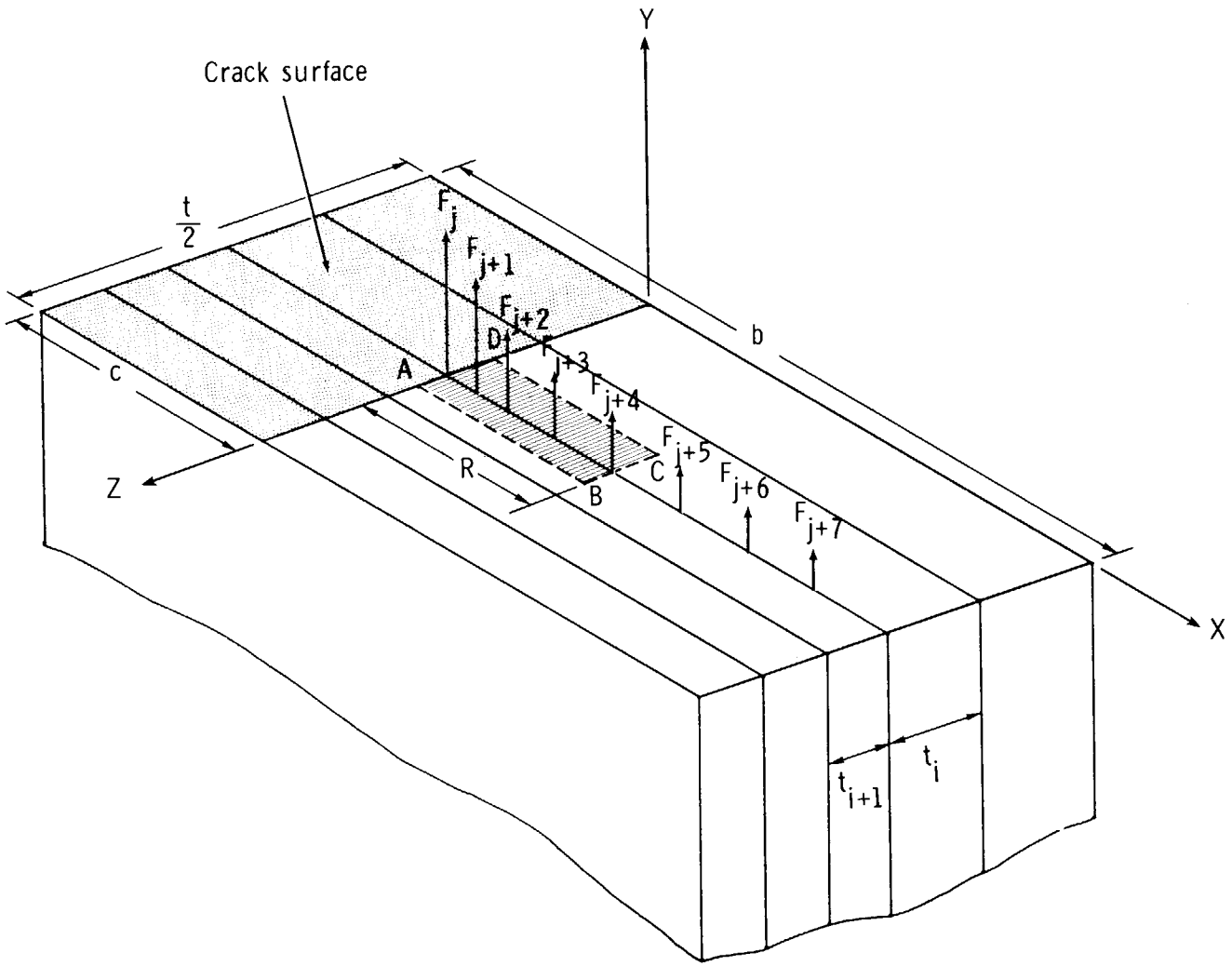

Figure 5.- Nodal forces on $Y = 0$ plane and at the interface between layers i and $i+1$.

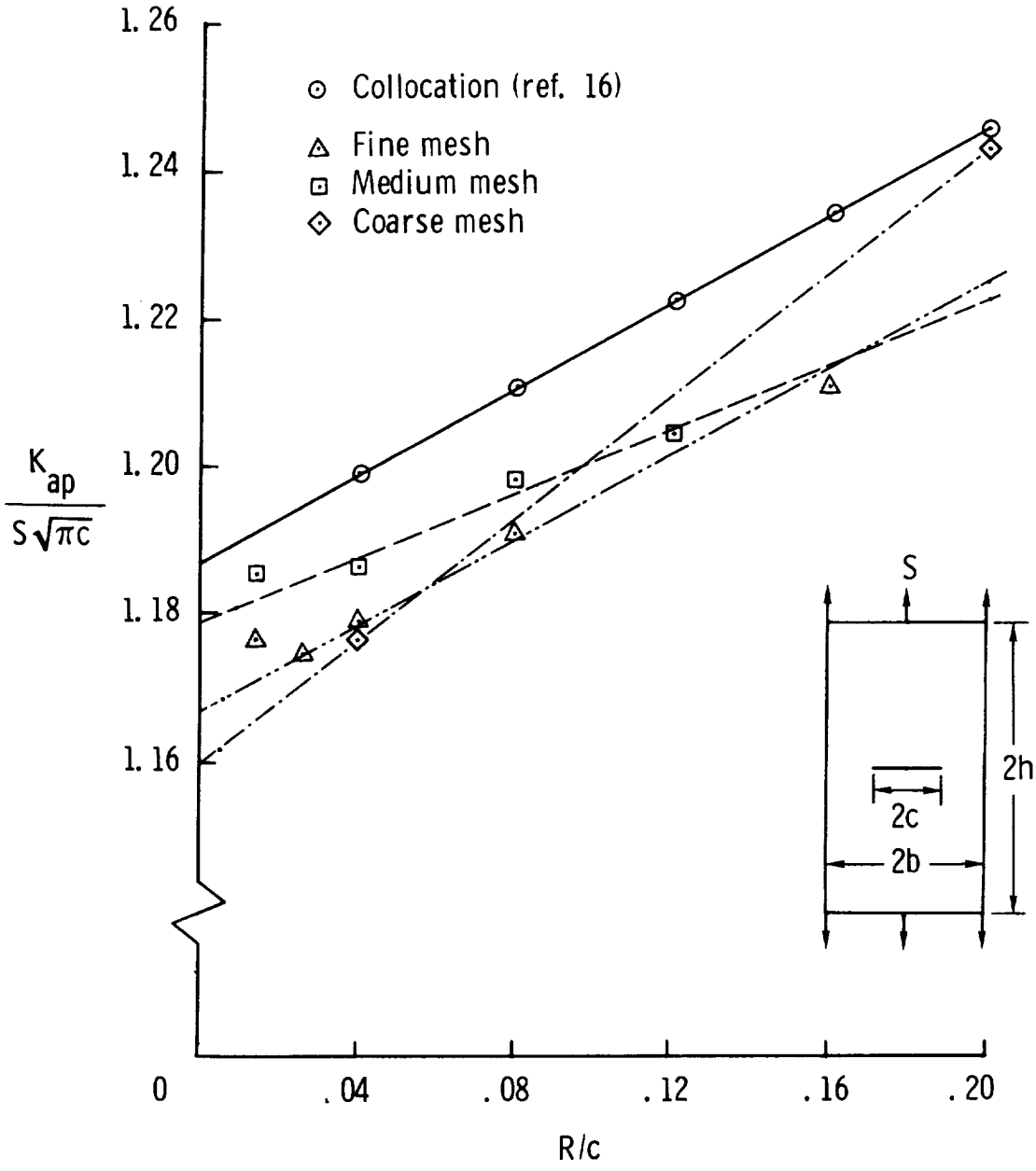

Figure 6.- Stress-intensity factor from two-dimensional analysis using force method for CCT specimen $\left(\frac{h}{b} = 3;\ \frac{c}{b} = 0.5\right)$.

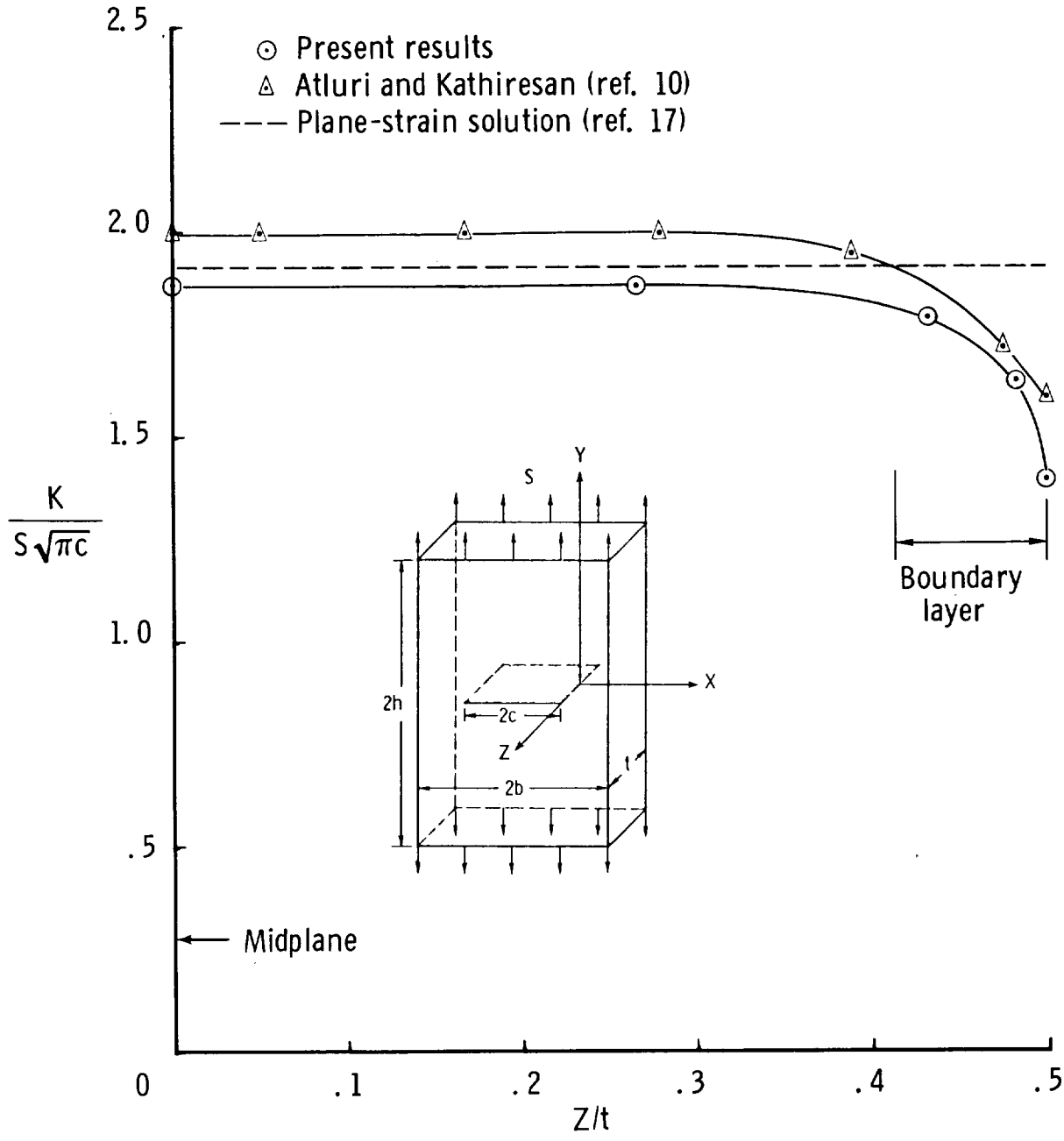

Figure 7.- Distribution of stress-intensity factor across thickness for CCT specimen $\left(\frac{h}{b} = 0.5;\ \frac{c}{b} = 0.5;\ \frac{t}{c} = 0.5;\ \nu = 0.3\right)$.

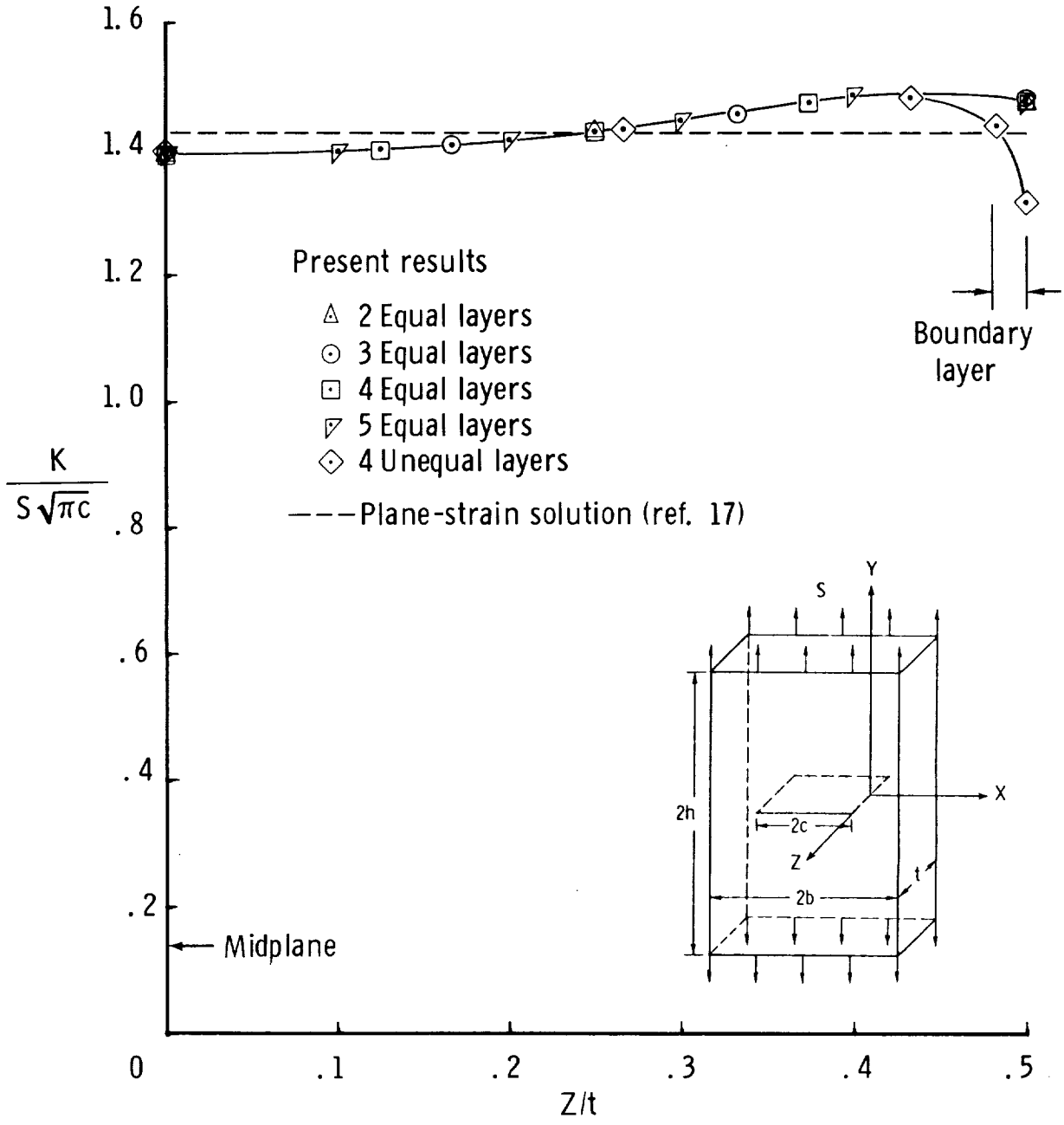

Figure 8.- Distribution of stress-intensity factor across thickness for CCT specimen for several models $\left(\frac{h}{b} = 0.875;\ \frac{c}{b} = 0.5;\ \frac{t}{c} = 3;\ \nu = \frac{1}{3}\right)$.

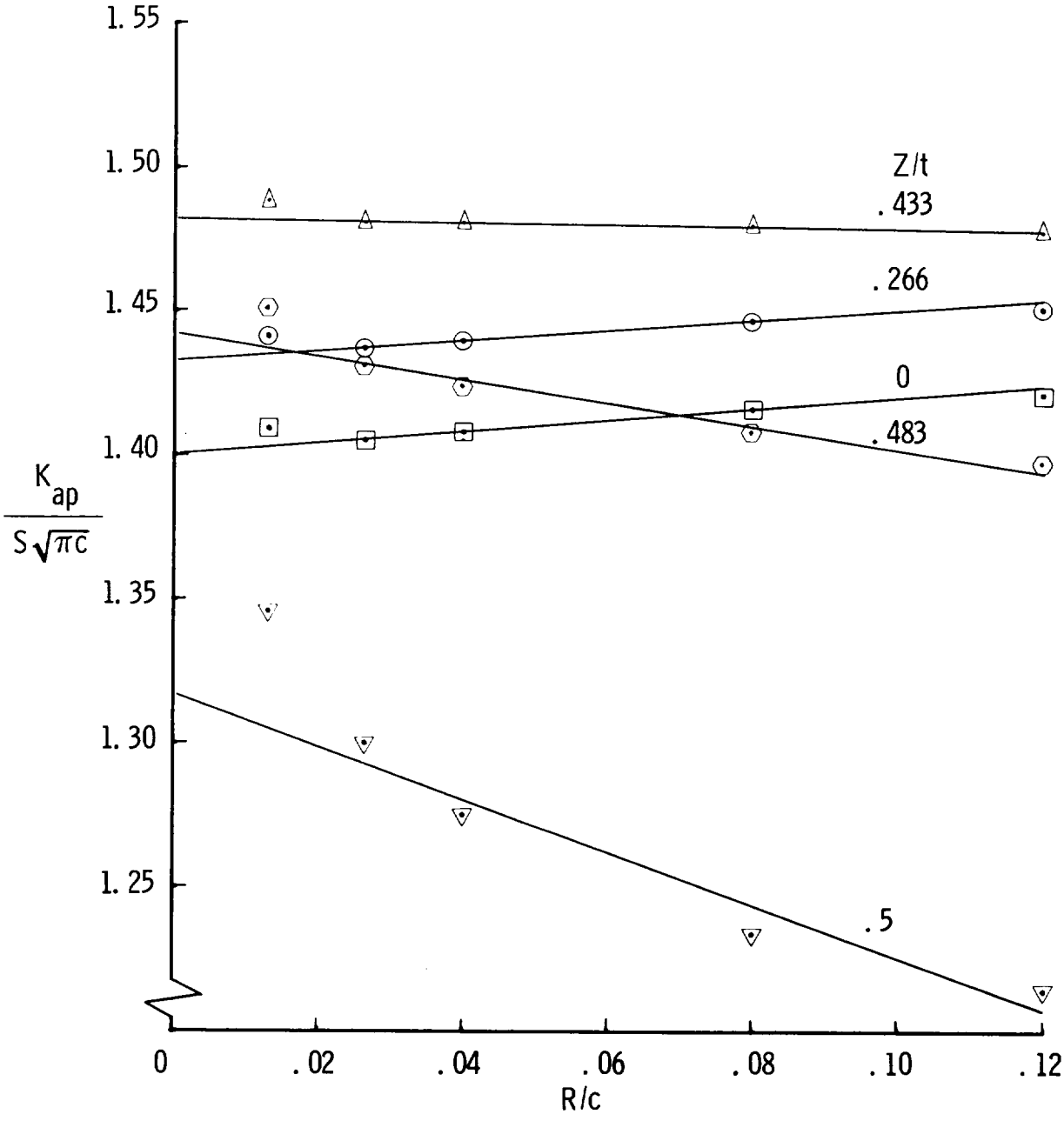

Figure 9.- Stress-intensity factor from three-dimensional analysis using force method for CCT specimen $\left(\frac{h}{b} = 0.875;\ \frac{c}{b} = 0.5;\ \frac{t}{c} = 3;\ \nu = \frac{1}{3}\right)$.

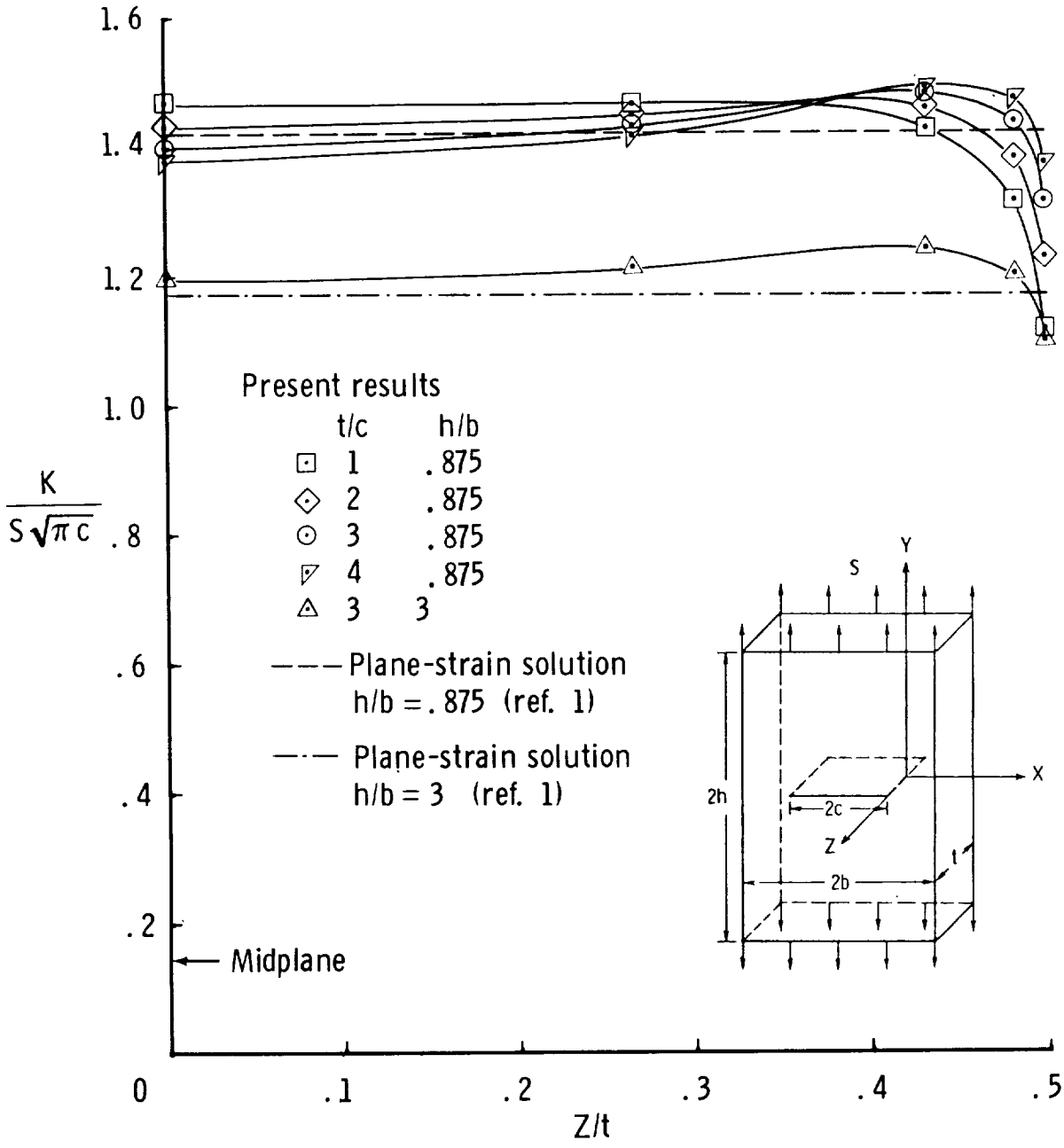

Figure 10.- Distribution of stress-intensity factor across thickness for CCT specimen as a function of t/c and h/b $\left(\frac{c}{b} = 0.5; \quad \nu = \frac{1}{3}\right)$.

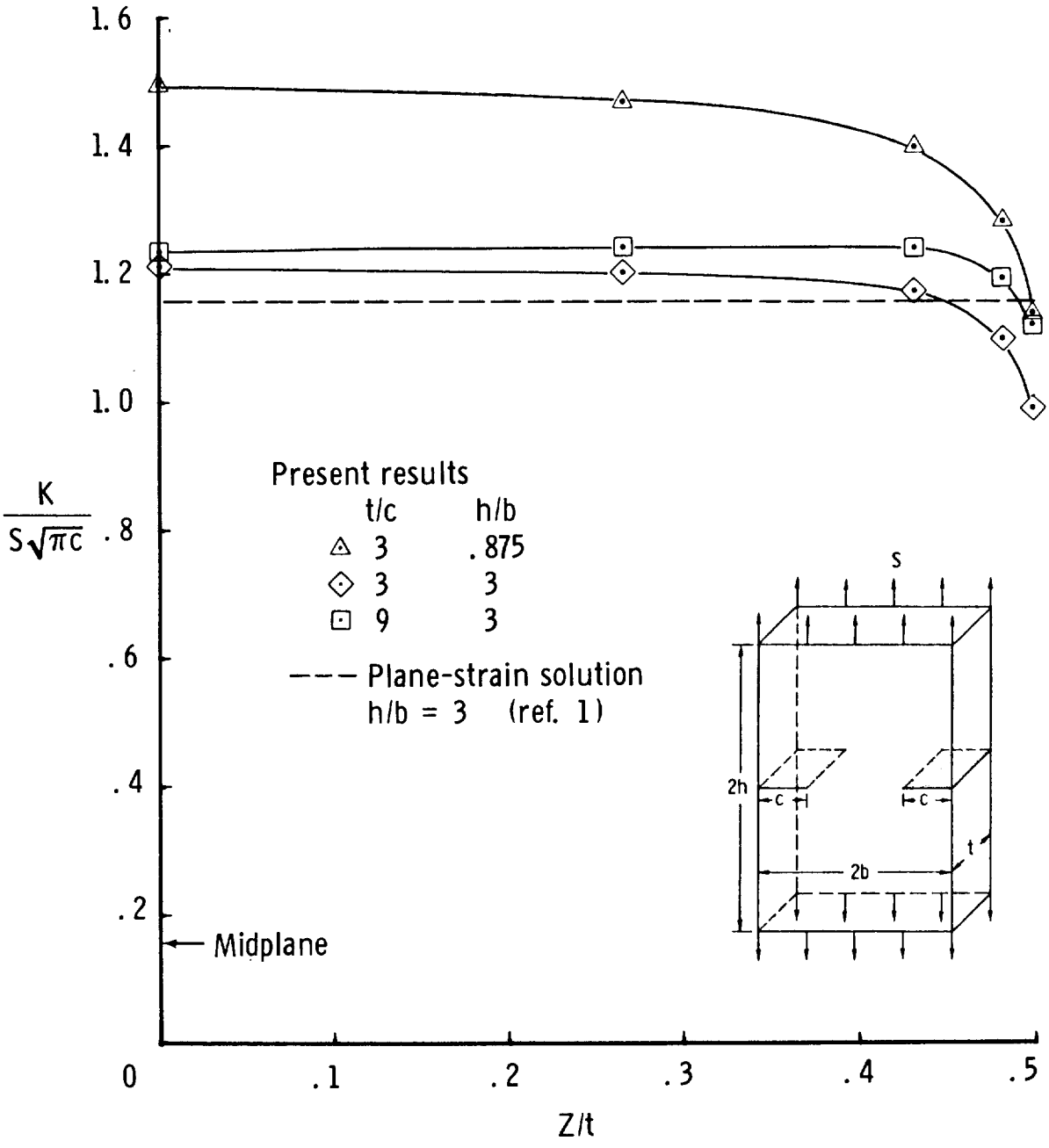

Figure 11.- Distribution of stress-intensity factor across thickness for DECT specimen $\left(\frac{c}{b} = 0.5; \quad \nu = \frac{1}{3}\right)$.

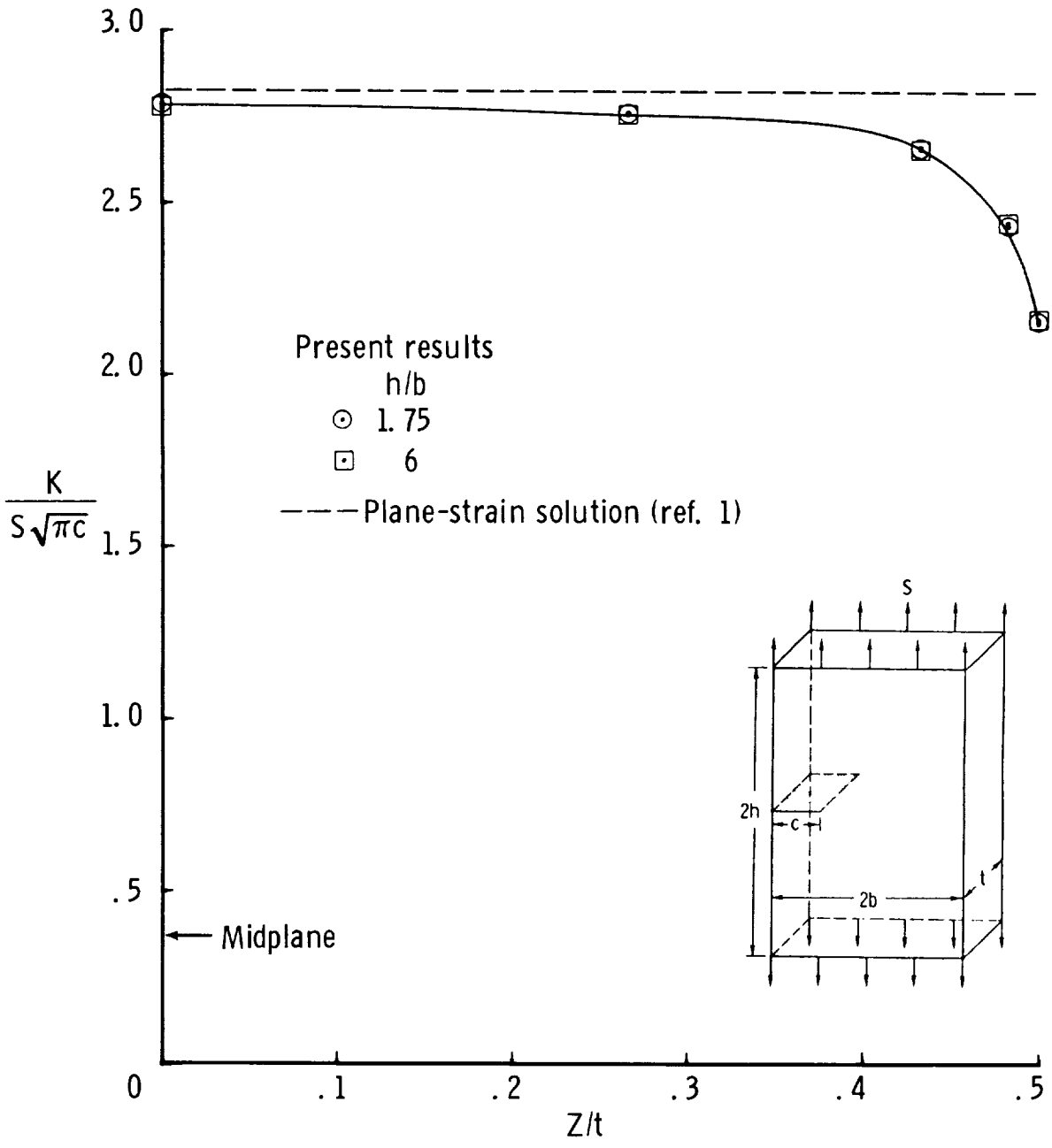

Figure 12.- Distribution of stress-intensity factor across thickness for SECT specimen $\left(\frac{c}{b} = 1.0;\ \frac{t}{c} = 3;\ \nu = \frac{1}{3}\right)$.

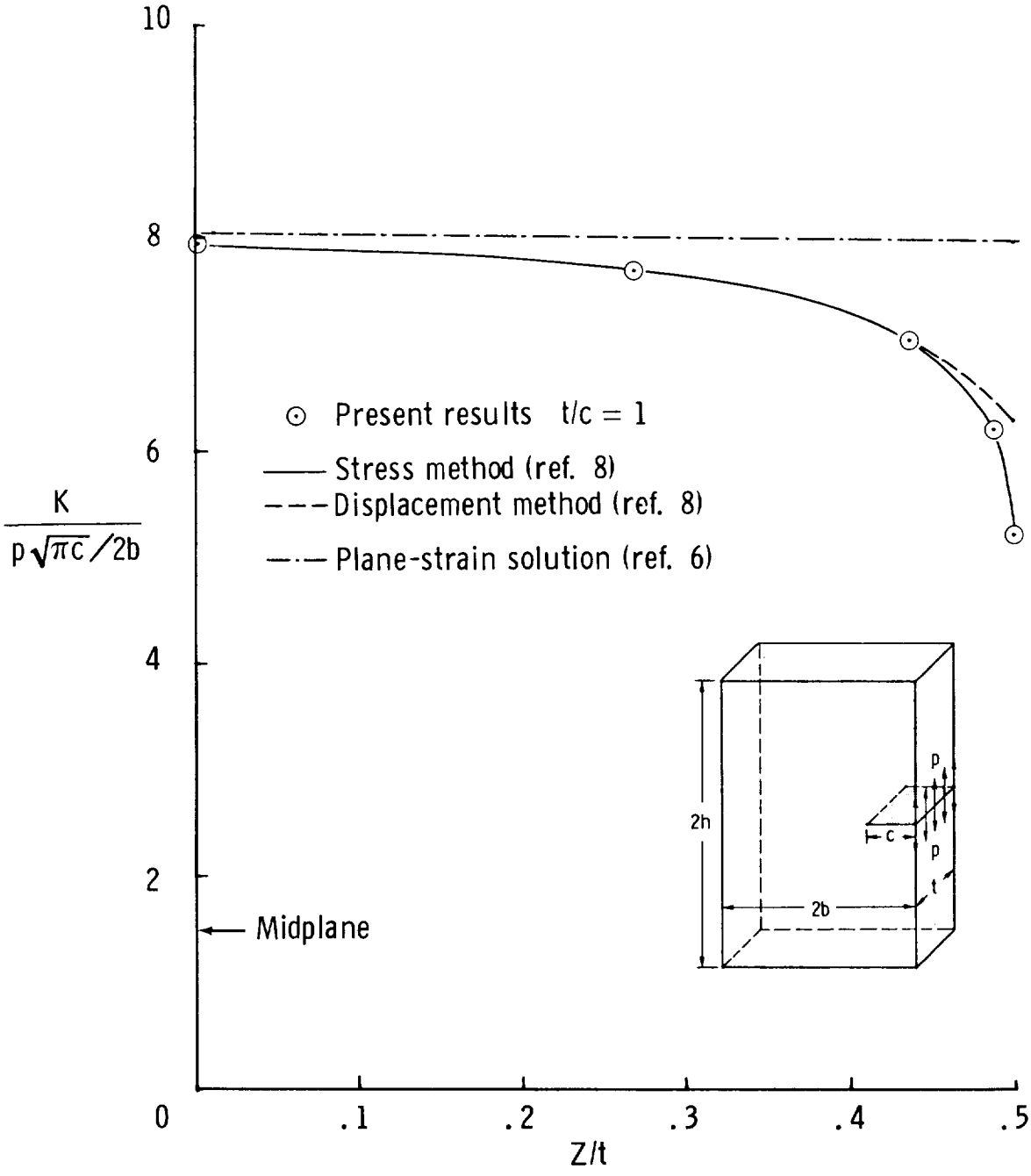

Figure 13.- Distribution of stress-intensity factor across thickness for compact specimen $\left(\frac{h}{b} = 1;\ \frac{c}{b} = 1;\ \frac{t}{c} = 1;\ \nu = 0.3\right)$.

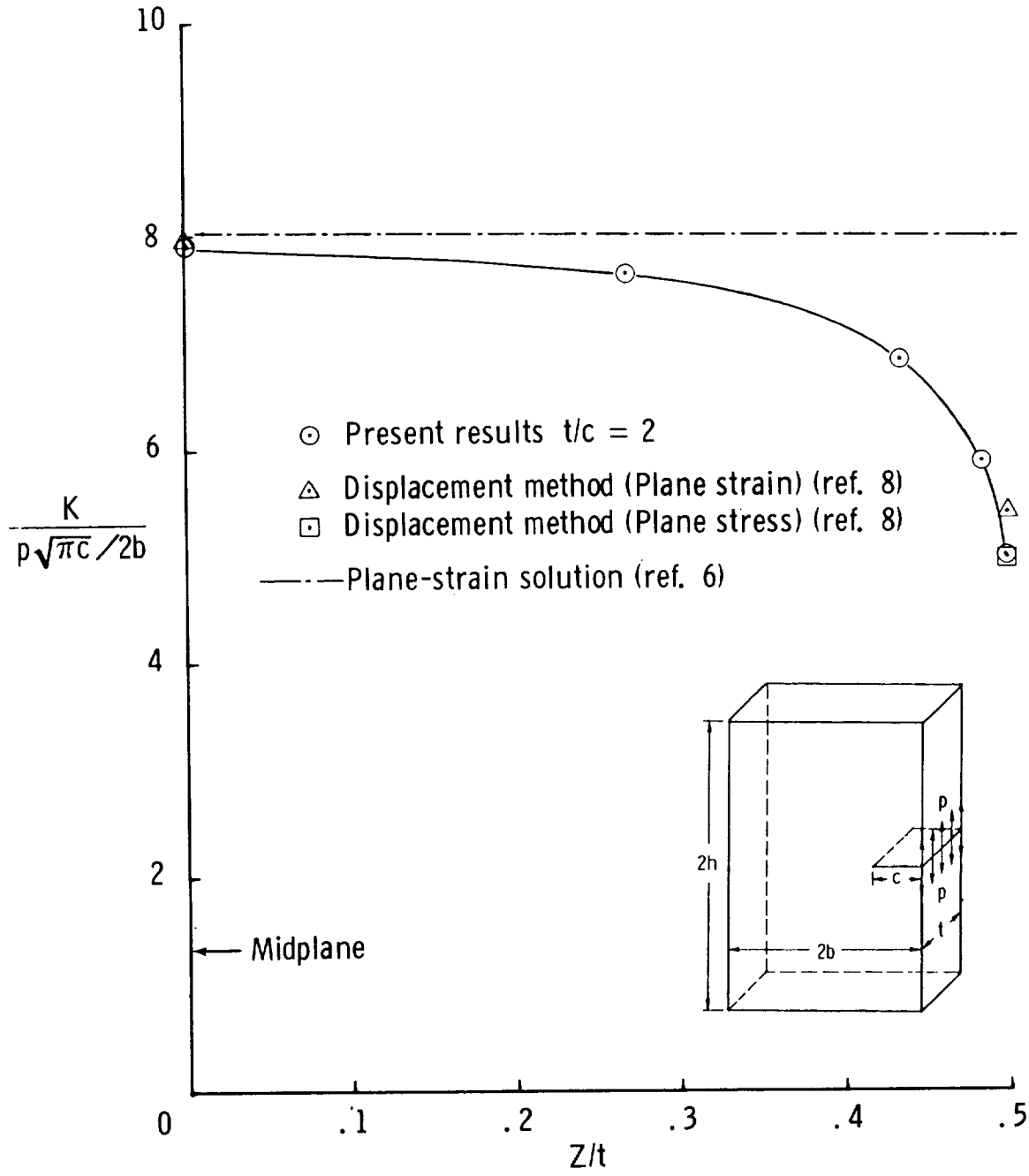

Figure 14.- Distribution of stress-intensity factor across thickness for compact specimen $\left(\frac{h}{b} = 1;\ \frac{c}{b} = 1;\ \frac{t}{c} = 2;\ \nu = 0.3\right)$.